Unidirectional Broadband Light Emission from Supported Plasmonic Nanowires

Timur Shegai,*,[†] Vladimir D. Miljković,[†] Kui Bao,[‡] Hongxing Xu,[§] Peter Nordlander,[‡] Peter Johansson,[†,‖] and Mikael Käll*,[†]

[†]Department of Applied Physics, Chalmers University of Technology, 412 96 Göteborg, Sweden
[‡]Department of Physics MS 61, Rice University, Houston, Texas 77005, United States
[§]Institute of Physics, Chinese Academy of Sciences, Box 603-146, 100190 Beijing, People's Republic of China
[‖]School of Science and Technology, Örebro University, 701 82 Örebro, Sweden

S *Supporting Information*

ABSTRACT: Metal nanowires are thought to become key elements in future nanophotonics applications. Here we show that single crystal silver nanowires supported on a dielectric interface behave similar to broadband unidirectional antennas for visible light. The degree of directionality can be controlled through the nanowire radius and its dielectric environment and the effect can be interpreted in terms of so-called leakage radiation from surface plasmons propagating in a single direction along a wire. We measure a forward-to-backward emission ratio exceeding 15 dB and an angular spread of 4° for wires with radii of the order 150 nm on glass in air. These findings could pave the way for development of metal nanowires as subwavelength directors of light in solar, sensor, and spectroscopy applications.

KEYWORDS: Nanowires, nanoantenna, directional emission, Fourier imaging
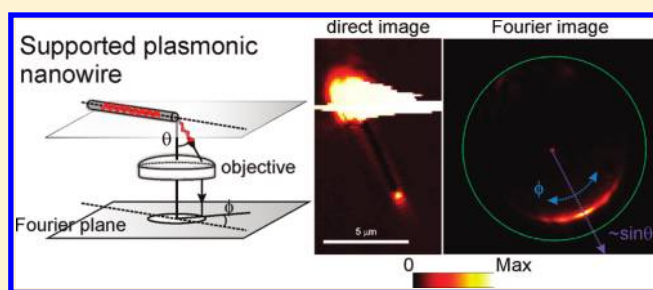
A classical unidirectional radio frequency (RF) antenna, for example, of the Yagi-Uda type, is designed for optimized reception of a narrowband signal incident from a particular direction.[1] The directionality originates from coupling between the different antenna elements, which have to be positioned such that interference is constructive in one direction and destructive in the opposite. By virtue of electromagnetic reciprocity, the antenna can also emit an RF signal in a directed manner if it is fed by a properly positioned source. A unidirectional antenna for visible light would fill similar needs as in the RF case, that is, to direct an optical signal from a subwavelength volume toward a well-defined direction or vice versa. Such a device could be of tremendous use for the development of novel optical sensors,[2,3] solar applications,[4] and molecular spectroscopy techniques, in particular if directionality could be achieved over a broad wavelength range.

It is well-known that certain subwavelength structures, in particular dimers of metal nanoparticles and bow-tie nanoantennas, are excellent for collecting and focusing light to nanometric volumes[5−9] with sufficiently large intensity enhancements to enable single-molecule Raman spectroscopy[6] and fluorescence.[10] But such structures are generally too small to provide significant phase retardation, which is a requirement for any kind of directional emission. Instead they radiate uniformly as Hertzian dipoles.[11] The recent development of directional optical antennas have therefore focused on RF inspired designs, that is, phase retardation engineering over length-scales dictated by the short wavelength of visible light.[12−16] However, the approach is technologically challenging and suffers from the intrinsic drawback that a device is engineered to operate within a small wavelength range. As an alternative, we here demonstrate that supported metal nanowires provide an efficient route toward unidirectional control of visible light at the nanoscale. We achieve directionality as high as 15 dB and an angular spread as narrow as 4° and 30° full width at half-maximum (fwhm) in the inclination and azimuthal directions, respectively. Moreover, broadband operation is possible because the nanowires support a broad continuum of propagating surface plasmon modes confined below the diffraction limit.[17−22] These results are important in the context of nanophotonics because metal nanowires are already known to be efficient nanoscale waveguides,[21,23] they can be made in large quantities using wet chemistry,[24] manipulated in solution,[25] and easily coupled to individual quantum emitters.[19]

Figure 1 illustrates the arrangement of the experiment and the principal observation. A silver nanowire immobilized on a glass slide is imaged in an inverted optical microscope by a high numerical aperture (NA) oil immersion objective. A laser beam ($\lambda = 632.8$ nm) is focused by the same objective at one end of the
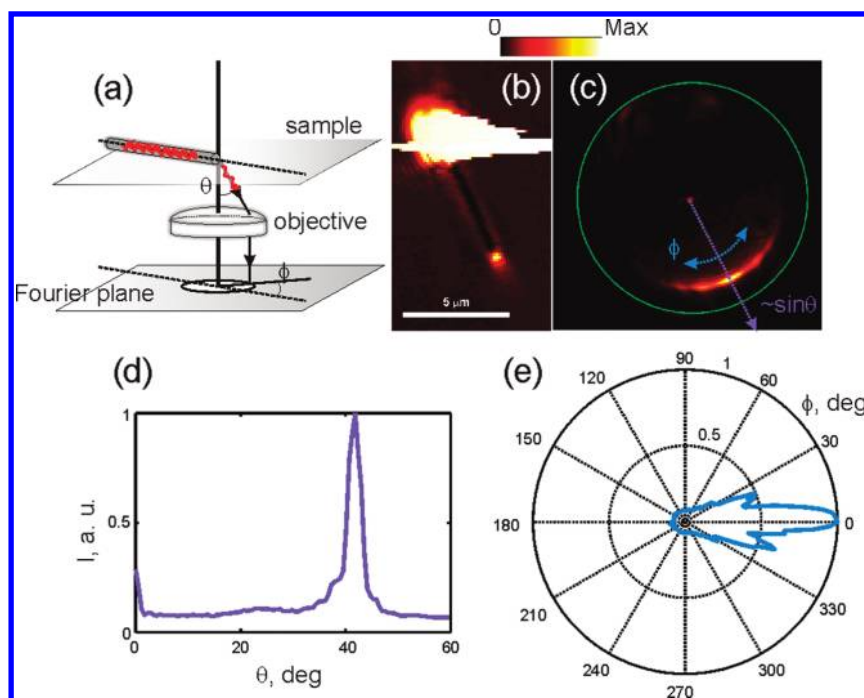
Figure 1. Unidirectional emission from a silver nanowire. (a) Illustration of the detection scheme and the coordinate system used. The nanowire is excited by a focused beam at the input end and the emitted light is detected in the Fourier plane of the optical microscope. (b) Direct optical image of a wire for λ = 632.8 nm excitation. (c) Corresponding Fourier image with the incident light blocked by an aperture in the image plane. (d) Emission intensity versus θ for ϕ = 0 and (e) versus ϕ for θ corresponding to maximum intensity.

nanowire, which we will refer to as the input end. With some efficiency, the incident photons are converted to plasmons that propagate along the wire toward the opposite end of the wire. The propagating plasmons are partly dissipated as heat due to Ohmic losses, partly reflected at the end of the wire, and partly coupled out to far field radiation.[17,21,22] The directionality of this emission is the first experimental problem that we address.

The angular distribution of the light intensity, $I = I(\theta, \phi)$, can be characterized by spherical angles θ and ϕ defined in Figure 1a and directly monitored in the Fourier plane of the microscope's objective. In practice, this is achieved by means of a 4f correlator scheme and by blocking the reflection from the incident radiation by a small aperture installed in the image plane of the microscope. A substantial part of the wire (usually several micrometers) contributes to the far-field intensity monitored in the Fourier plane. The radial coordinate on the Fourier image scales as the numerical aperture NA = $n \sin \theta$, where n = 1.52 is the refractive index (RI) of the glass substrate, while the tangential coordinate corresponds to the angle ϕ ($0 < \phi < 2\pi$). The green circle in Figure 1c represents NA = 1.3, the maximum NA of the 100× oil immersion objective used for this experiment. From panel d, we read that the intensity peaks sharply around $\theta_{max} \approx 42°$. This angle is very close to the critical angle of the air–glass interface, defined as $\theta_c = \arcsin(1/n_{glass}) = 41.5°$. From Figure 1b,c,e, it is clear that the orientation of the nanowire coincides with the direction for which most light is observed in the Fourier plane (we choose ϕ = 0 to be along the wire), although we also observe secondary and tertiary maxima at angles away from ϕ_{max}. Most important, however, is that there is essentially no light observed in the backward direction ($\phi = \phi_{max} \pm 180°$), that is, the wire exhibits unidirectional emission.

The observation that the emission peaks close to $\theta = \theta_c$ suggests that the RI contrast between the substrate supporting

the nanowire and the medium around it has a crucial impact on the directionality. To experimentally check if this is the case, we performed a series of experiments in which we decreased the RI mismatch between the glass substrate and the surrounding medium. The wires were first immobilized on the air–glass interface and then successively immersed in water (n = 1.33), ethylene glycol (EG) (n = 1.42) and index matched oil (n = 1.515) while the emission pattern was studied using an ultra-high NA objective (60×, NA = 1.49). We excited the input end of the wires in the same way as in Figure 1 but now using white light to reveal potential color dispersion in the emission patterns and to be able to record spectra. The diameters of the wires were estimated by comparing their optical contrasts with standards cross-checked with scanning electron microscopy (SEM) images (see Supporting Information Figure S1). Figure 2 summarizes results for representative "thin" and "thick" wires with estimated diameters of the order 90 ± 20 and 320 ± 35 nm, respectively. Focusing first on the "thick" wire in air, it is immediately clear that the narrow (fwhm = 4°) emission around θ_c in the direction ϕ = 0 seen in Figure 1 is preserved for white light excitation. This result was checked for several thick wires using color filters in the beam path, but no dispersion could be detected within the experimental accuracy and wavelength range investigated. Evidently, "thick" silver nanowires function similar to narrow unidirectional broadband antennas! Moreover, as is obvious from the intensity plots in Figure 2b, the direction of the emission tracks the critical angle of the interface that supports the wire, thus offering a simple means of directional tuning through RI contrast. A quite different behavior is found for the "thin" wire. Most importantly, the wire now radiates in a broader set of angles and a noticeable fraction of the emitted light is sent out in the backward direction at around $\theta = -\theta_c$. Moreover, the overall intensity of the emission is about an order of magnitude lower than for the thick wire. We define a
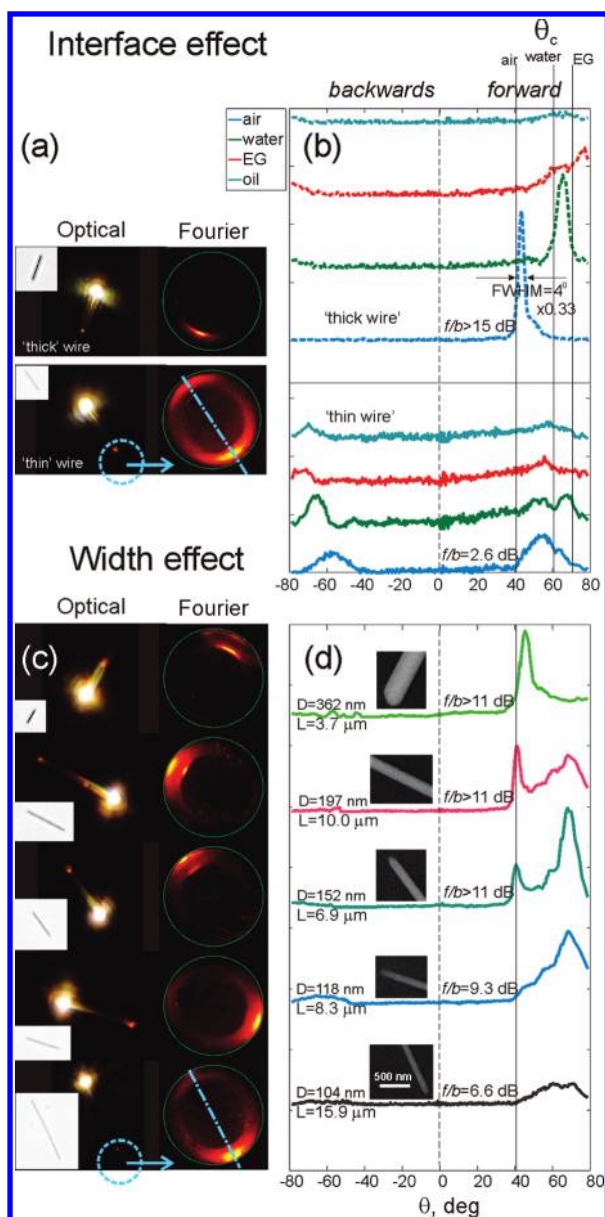
Figure 2. Experimental demonstration of angular tuning by a change in (a,b) the refractive index contrast between the glass substrate and the immersing medium and (c,d) the wire width. The strongest unidirectionality is obtained for thick wires in air. All results are for white light excitation. Panels a,c show direct optical images (wide-field illumination in gray scale, focused illumination in color), scanning-electron microscopy images, and Fourier images of wires of different dimensions. The wire diameters given in (a) are estimates based on the optical contrast. The dashed blue circles indicate the area used for Fourier imaging. Panels b,d show emission intensity vs θ for $\phi = 0$ (indicated by blue dash-dotted lines for two of the wires). Forward emission corresponds to $\theta > 0$ and backward to $\theta < 0$. The vertical lines indicate the critical angles θ_c in the different immersion media (air, water, and ethylene glycol).

quantitative measure of the emission directionality as a forward-to-backward ratio measured in dB ($f/b = 10 \log(I_f/I_b)$). For the case of the thin wire, the directionality is about 2.6 dB, while in the case of the thick wire, there is virtually no photons observed in the backward direction and the f/b ratio is only limited by the noise level. We thus can safely estimate the directionality to exceed 15 dB in this case. The thickness of a

nanowire is thus a critical parameter in the observed unidirectionality phenomenon. To study the influence of the wire diameter more quantitatively, we performed a set of experiments on air—glass interfaces, so that the wires could be imaged in SEM after recording all the optical information. The results for the wire width effect are summarized in Figure 2c,d. Wires in the range of diameters between about 100—360 nm were studied. For $D = 104$ nm, we observe a behavior that is very similar to a representative thin wire, namely the wire radiates preferably in the forward direction at a range of angles between 40 and 80°. On the other hand for $D = 362$ nm wire, we observe an extremely unidirectional ($f/b > 11$ dB close to θ_c) radiation pattern, which is also in line with observations for the representative thick wire. For intermediate thick wires (100 nm $< D <$ 200 nm), we observe both a sharp peak at $\theta = \theta_c$ and a broader peak at bigger angles, the relative contribution of which depends on the exact value of the diameter. Thus, we also observe a transition from a characteristic thin wire to a characteristic thick wire behavior.

To understand the basic origins of the unidirectional wire emission, let us first consider radiation from an oscillating point dipole near a planar interface. In contrast to a dipole in a homogeneous medium, a dipole on a substrate essentially emits a cone of light with maxima at the critical angle due to conversion of evanescent waves above the interface to propagating waves in the optically dense medium.[26,27] Light radiated at angles below the critical is referred as "allowed" and the light above correspondingly as "forbidden". Fourier images of dipole radiation above a surface are shown in Supporting Information Figure S2. From the figure, it is clear that a single dipole cannot generate unidirectional emission. To establish directional control, the symmetry has to be broken further by extending from a single dipole source to a chain of dipoles with internal phase retardation corresponding to a wave traveling in one direction. This is demonstrated in Supporting Information Figure S3 for a chain of 10 point dipoles. Although the exact radiation pattern depends on geometrical parameters, there is clearly a striking similarity between the simulated Fourier images and the ones shown in Figures 1 and 2 for the thick wires. Naturally, unidirectionality is lost by symmetry if the chain of dipoles instead would oscillate as if driven by two equal waves traveling in opposite directions. These observations allow us to explain the observed directionality effects in the following simple terms:

In the case of thick wires, light is emitted along the length of the wire by a charge density oscillation propagating from the input end toward the distant part of the wire, in other words a surface plasmon. However, because of high propagation losses to radiation and heat, there is essentially no plasmon wave traveling in the opposite direction. Hence, light emission is unidirectional. In contrast, in the case of thin wires we have less radiative losses and therefore lower overall emission intensity, which is in line with the data in Figure 2. Thus, the reflected plasmon amplitude propagating back from the wire-end will be significant, resulting in a much more symmetric radiation pattern. We should point out that for neither the thin or thick wire is the sharp cone of light seen in the Fourier images around θ_c due to emission from only the tip at the end of the wires, as could be suggested by the bright wire tips in the optical images, but due to light emission from the entire length of the wire.

To experimentally verify the scenario above, we performed two additional experiments. First, we translated wires in relation to the aperture used to block the incident light. The intensity in
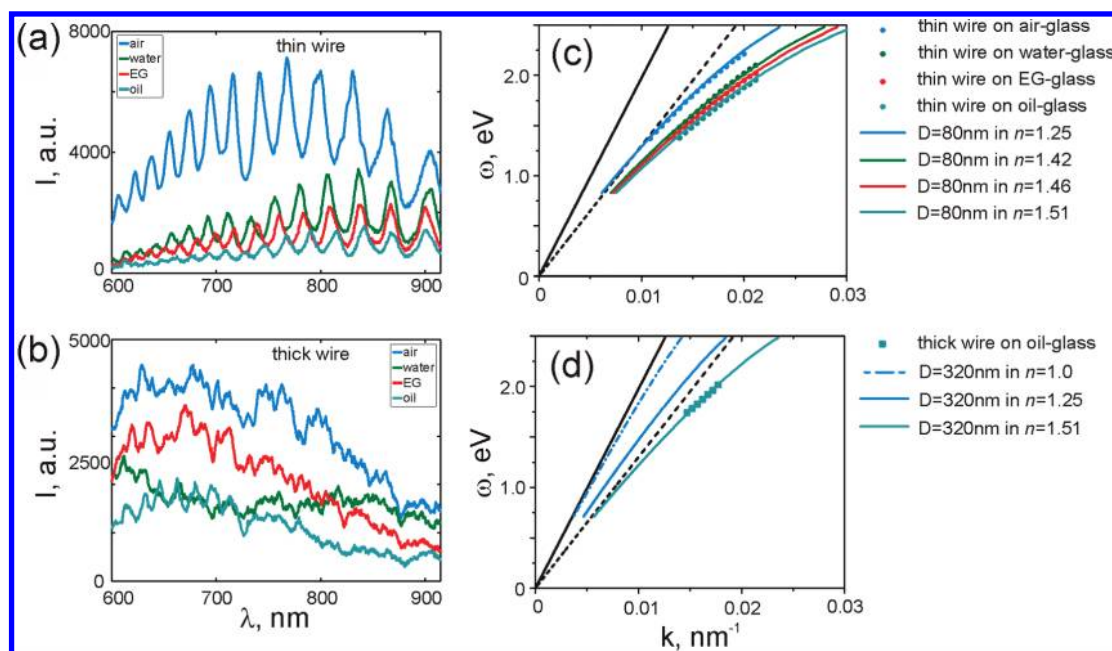
Figure 3. Emission spectra and plasmon dispersion relations of thin and thick silver nanowires as a function of refractive index contrast. The thin wire exhibits pronounced FP resonances (a) and dispersion curves that fall below the light lines of the surrounding media (c). In contrast, the pronounced unidirectionality observed for thick wires is associated with poorly defined emission spectra (b) and leaky surface plasmons (d). The dispersion relations were estimated experimentally (points) from emission spectra using the FP model and calculated analytically using the infinite metal cylinder model (lines). Black lines in panels c and d show light dispersion in air (solid) and glass (dash), respectively.

the directional lobes in the Fourier plane was found to be roughly proportional to the fraction of the wire length selected by the aperture (see Supporting Information Figures S4). Thus, the directional emission must emerge from the entire length of the wires. Second, we investigated the spectral properties of the wire emission. As first shown by Krenn and co-workers, high quality silver nanowires act as plasmonic Fabry−Perot (FP) resonators.[21] This means that the emission spectrum from a particular wire will be modulated according to its length and the wavelength and decay-length of the plasmons it support. Wires with low losses should then exhibit high quality FP resonances but be less unidirectional, and vice versa. The spectra in Figure 3 (measured from the same wires as in Figure 2) show that this is indeed the case. The thin wire exhibits sharp spectral peaks, corresponding to a high quality FP cavity, while the thick wire spectra exhibit much less distinct modes.

The results above can also be discussed in the framework of ordinary surface plasmon in thin metal films. Notice first that each peak in a wire spectrum corresponds to a standing wave resonance determined by the particular dispersion curve $\omega(k_{SP})$ for that wire.[21,28−32] We can reconstruct approximate dispersion relations for a given wire based on the FP model (see section Fabry−Perot resonator and infinite metal cylinder model in Supporting Information) and by comparing with theoretical dispersion relations for infinite cylinders.[33,34] We then assume that the thin and thick wires have diameters of 80 and 320 nm, respectively (which falls well within the diameters estimated from the optical contrast), and that they are situated in homogeneous environments characterized by an RI that is the average between the substrate and the actual immersing medium. As seen in Figure 3c,d, this leads to the interesting prediction that the dispersion curves for the thin wire are expected to fall below the "light line" for the glass substrate, meaning that the plasmons momenta are too large to allow for plasmon decay into far field photons. In the case of the thick wire, in contrast, the calculations

predict that the plasmon dispersion should fall well above the light line in glass. Thus, the thick wire plasmons are "lossy" and will have a short decay length, thereby enabling unidirectional emission into the substrate.

To provide additional information on the wire emission process, we performed electrodynamics simulations of near-field and far-field optical properties for $\lambda = 632.8$ nm. The computational complexity forced us to combine several different calculation methods and to focus on wires with diameters below 160 nm. Figure 4a,b shows COMSOL simulations of near-field patterns for thin ($D = 80$ nm) and comparatively thick ($D = 160$ nm) silver wires, respectively, situated on finite glass substrates and excited by a Gaussian beam at the "input end". Importantly, the resulting standing wave pattern for the thick wire exhibit clearly longer plasmon wavelength (smaller k_{SP}) at the upper (air) than at the lower (glass) side. A wire in a homogeneous background possesses modes with cylindrical symmetry characterized by an azimuthal quantum number m, but this symmetry is lost here and the wire instead supports an "airlike" and a "glasslike" hybridized plasmon. These modes mainly derive from the $m = 0$ and $m = 1$ modes of a wire in a uniform background. Although both modes can be excited by the incident focused radiation, the airlike leaky plasmon is the main source of radiation into the glass substrate. In fact, one can see how the intensity of the field diminishes faster along the top of the wire than along the bottom in Figure 4b. The thin wire, in contrast, exhibits an extremely uniform standing wave pattern all along its length, as expected for a high quality plasmon FP cavity. Finally, Figure 4c,d shows simulations of far-field emission obtained by the Green's function method for stratified media.[35,36] We investigated wires with the same diameters as above, but the wire lengths had to be shortened from 5 to 2 μm due to computational constraints. We simulated the aperture used to block the incident light by only including emission from the final 1.5 μm of wire length in
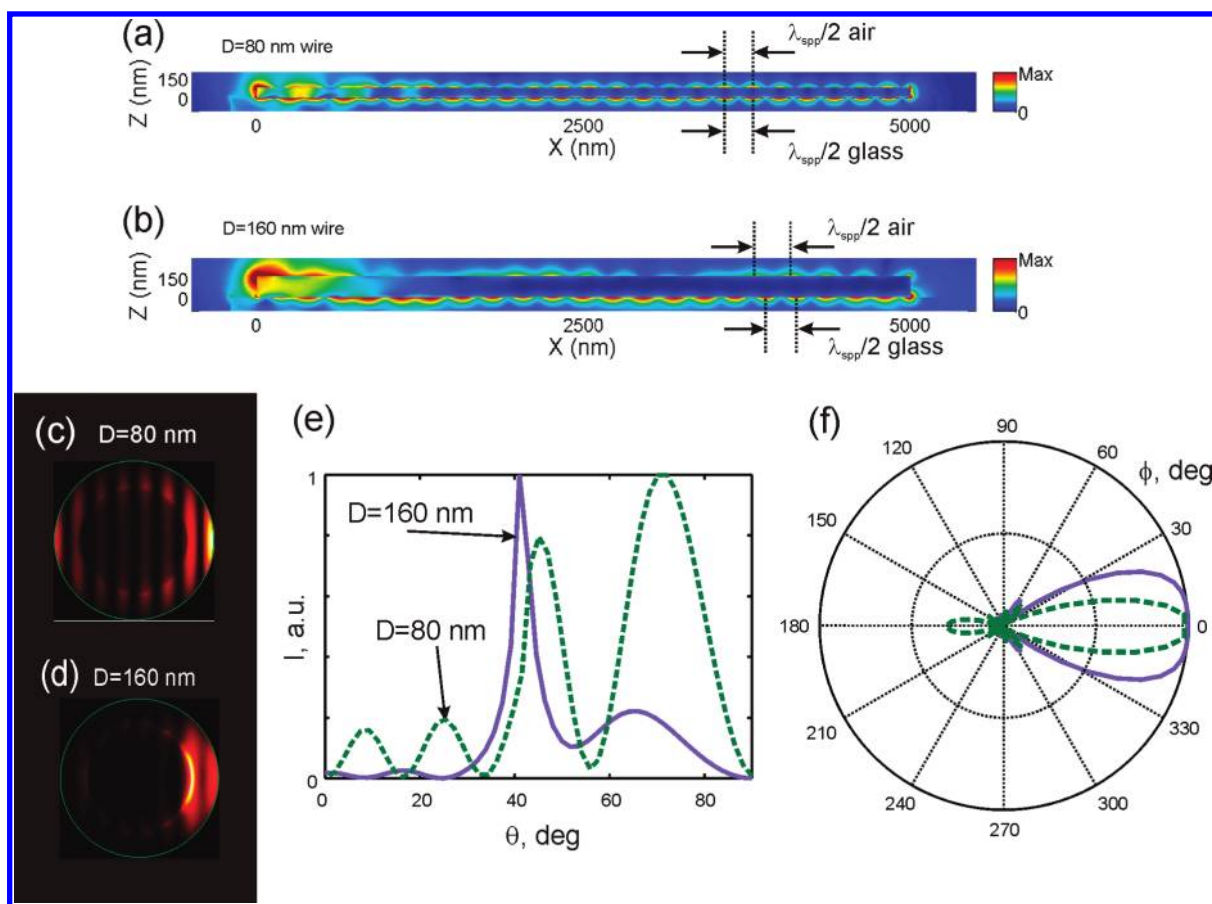
Figure 4. Electrodynamics simulations of near-field and far-field emission patterns for thin ($D = 80$ nm) and thick ($D = 160$ nm) silver nanowires at $\lambda = 632.8$ nm. (a,b) Near-field intensity maps $|E|^2$ for 5 μm long wires on an air-glass interface computed using COMSOL. (c,d) Corresponding Fourier images obtained using the Green's function method for wires of length 2 μm. (e,f) The emission intensity versus θ for $\phi = 0$ and vs ϕ for θ corresponding to maximum intensity, respectively. Note the close agreement with the angular plots in Figures 1 and 2.

the calculated far-field Fourier transform images. It is clear that the simulations reproduce the essential details of the experiment, in particular the unidirectionality effect and the sharp emission near θ_c for the thick wire. Notice also the "antenna lobes" in Figure 4f, which are similar to the ones in Figure 1. These are due to interference and arise because only a finite number of standing wave nodes contribute to the far-field.

In conclusion, we have demonstrated highly unidirectional broadband light emission from supported plasmonic nanowires. The phenomenon can be discussed in terms of so-called leakage radiation from surface plasmons on metal films. However, the ultimate cause of the effect can be traced back to the emission from a chain of dipoles with appropriate relative phase retardation, situated above an interface. In this sense, the origin of directionality here is similar to that in a phased array or Yagi-Uda antenna, although retardation in the present case is dictated by the nanowire diameter and dielectric environment according to the plasmon dispersion relation. This offers a high degree of tunability and suggests novel applications, such as directional surface plasmon resonance biosensing and surface-enhanced spectroscopy at the nanoscale.

Methods. High-quality silver nanowires were prepared using a wet chemistry method described by Sun et al.[24] The wires were attached to microscope glass slides (25×25 mm) functionalized with polylysine (0.25 mg/mL for 10 min) by allowing them to adsorb for about 1 min, after which the slide was thoroughly washed with deionized water and dried in nitrogen.

Optical excitation of the wires was performed using a linearly polarized 632.8 nm He−Ne laser beam or using unpolarized white light. The sample was mounted on XY stage of an inverted microscope equipped with an oil immersion objectives ($100\times$ NA = 1.3 or $60\times$ NA = 1.49). The excitation light was focused by the objective on the input end of the wire and the light reemitted by the wire was collected in a backscattering geometry. We blocked the incident radiation from reaching the image sensor by placing an iris in the image plane of the microscope. Fourier images were obtained by means of an achromatic 4f correlator scheme while wire spectra were recorded by a fiber coupled grating spectrometer.

Near-field calculations were done using the commercial finite element method COMSOL and with the Ag wire placed on a finite 6 μm $\times$ 800 nm $\times$ 200 nm glass slab. Radiation patterns were calculated with the Green's function method using cubic mesh elements of side 5 nm. Excitation was limited to the last 300 nm of the input wire end.

■ ASSOCIATED CONTENT

ⓢ Supporting Information. Figures with additional text and formulas. This material is available free of charge via the Internet at http://pubs.acs.org.

■ AUTHOR INFORMATION

Corresponding Author

*E-mail: (T.S.) timurs@chalmers.se; (M.K.) kall@chalmers.se.

■ ACKNOWLEDGMENT

■ REFERENCES

(1) Stutzman, W. L.; Thiele, G. A. *Antenna theory and design*; Wiley: New York, 1981.

(2) Lal, S.; Link, S.; Halas, N. J. *Nat. Photonics* **2007**, *1*, 641.

(3) Anker, J. N.; et al. *Nat. Mater.* **2008**, *7*, 442–453.

(4) Atwater, H. A.; Polman, A. *Nat. Mater.* **2010**, *9*, 205–213.

(5) Muhlschlegel, P.; Eisler, H. J.; Martin, O. J. F.; Hecht, B.; Pohl, D. W. *Science* **2005**, *308*, 1607–1609.

(6) Xu, H. X.; Bjerneld, E. J.; Käll, M.; Borjesson, L. *Phys. Rev. Lett.* **1999**, *83*, 4357–4360.

(7) Schuck, P. J.; Fromm, D. P.; Sundaramurthy, A.; Kino, G. S.; Moerner, W. E. *Phys. Rev. Lett.* **2005**, *94*, No. 017402.

(8) Schnell, M.; et al. *Nat. Photonics* **2009**, *3*, 287–291.

(9) Lezec, H. J.; et al. *Science* **2002**, *297*, 820–822.

(10) Kinkhabwala, A.; et al. *Nat. Photonics* **2009**, *3*, 654–657.

(11) Huang, C.; et al. *Phys. Rev. B* **2008**, *78*, No. 155407.

(12) Alaverdyan, Y.; Sepulveda, B.; Eurenius, L.; Olsson, E.; Käll, M. *Nat. Physics* **2007**, *3*, 884–889.

(13) Taminiau, T. H.; Stefani, F. D.; Segerink, F. B.; Van Hulst, N. F. *Nat. Photonics* **2008**, *2*, 234–237.

(14) Pakizeh, T.; Käll, M. *Nano Lett.* **2009**, *9*, 2343–2349.

(15) Kosako, T.; Kadoya, Y.; Hofmann, H. F. *Nat. Photonics* **2010**, *4*, 312–315.

(16) Curto, A. G.; et al. *Science* **2010**, *329*, 930–933.

(17) Shegai, T.; Huang, Y. Z.; Xu, H. X.; Käll, M. *Appl. Phys. Lett.* **2010**, *96*, No. 103114.

(18) Li, Z. P.; et al. *Nano Lett.* **2009**, *9*, 4383–4386.

(19) Akimov, A. V.; et al. *Nature* **2007**, *450*, 402–406.

(20) Falk, A. L.; et al. *Nat. Physics* **2009**, *5*, 475–479.

(21) Ditlbacher, H.; et al. *Phys. Rev. Lett.* **2005**, *95*, No. 257403.

(22) Yan, R. X.; Pausauskie, P.; Huang, J. X.; Yang, P. D. *Proc. Natl. Acad. Sci. U.S.A.* **2009**, *106*, 21045–21050.

(23) Cai, W.; Sainidou, R.; Xu, J. J.; Polman, A.; de Abajo, F. J. G. *Nano Lett.* **2009**, *9*, 1176–1181.

(24) Sun, Y. G.; Xia, Y. N. *Adv. Mater.* **2002**, *14*, 833–837.

(25) Tong, L. M.; Miljkovic, V. D.; Käll, M. *Nano Lett.* **2010**, *10*, 268–273.

(26) Lieb, M. A.; Zavislan, J. M.; Novotny, L. *J. Opt. Soc. Am. B* **2004**, *21*, 1210–1215.

(27) Novotny, L.; Hecht, B. In *Principles of Nano-Optics*; Cambridge University Press: New York, 2006; pp 335−362.

(28) Dorfmuller, J.; et al. *Nano Lett.* **2009**, *9*, 2372–2377.

(29) Barnard, E. S.; White, J. S.; Chandran, A.; Brongersma, M. L. *Opt. Express* **2008**, *16*, 16529–16537.

(30) Sondergaard, T.; Bozhevolnyi, S. I. *Phys. Status Solidi B* **2008**, *245*, 9–19.

(31) Sondergaard, T.; Beermann, J.; Boltasseva, A.; Bozhevolnyi, S. I. *Phys. Rev. B* **2008**, *77*, No. 115420.

(32) Gomez-Medina, R.; Yamamoto, N.; Nakano, M.; Abajo, F. J. G. *New J. Phys.* **2008**, *10*, No. 105009.

(33) Novotny, L. *Phys. Rev. Lett.* **2007**, *98*, No. 266802.

(34) Novotny, L.; Hafner, C. *Phys. Rev. E* **1994**, *50*, 4094–4106.

(35) Martin, O. J. F.; Dereux, A.; Girard, C. *J. Opt. Soc. Am. A* **1994**, *11*, 1073–1080.

(36) Johansson, P. *Phys. Rev. B* **2010**, submitted for publication; http://arxiv.org/abs/1012.0792.